Ab initio lattice dynamics and electron-phonon coupling in Li_xZrNCl

R. Heid* and K.-P. Bohnen
Forschungszentrum Karlsruhe, Institut für Festkörperphysik, D-76021 Karlsruhe, Germany
(Received 6 July 2005; published 28 October 2005)

Transition metal chloronitrides represent a class of layered compounds, which after intercalation, become superconductors with T_c's up to 25.5 K. We present a theoretical investigation of the phonon dispersions and electron-phonon coupling for the undoped and Li-doped ZrNCl, which is one prominent representative of this class of materials. The calculations are based on density functional perturbation theory in the framework of the mixed-basis pseudopotential method. For the undoped parent compound β-ZrNCl, we are able to identify all structures in the measured phonon-density of states. For the doped system, the partial occupation of the Li site is treated by an artificial doping approach. Doping partially fills a quasi-2D conduction band and gives rise to almost cylindrical Fermi surfaces around the zone boundary K point. The doping induced electron-phonon coupling is also very 2D-like and exhibits a strong momentum-dependent renormalization involving selective phonon modes of in-plane vibrations of Zr and N. Although there is a larger coupling to the higher-frequency N vibrations, the average coupling constant is only ≈ 0.5. Within the standard Eliashberg analysis in the dirty limit, the calculated electron-phonon coupling is too weak to explain the observed T_c. Our results point to the need for a more accurate treatment of the Coulomb screening effects in these highly anisotropic layered superconductors.

DOI: 10.1103/PhysRevB.72.134527 PACS number(s): 74.70.Dd, 63.20.Dj, 63.20.Kr, 71.15.Mb

I. INTRODUCTION

The transition metal chloronitrides MNCl (M=Zr, Hf) constitute an interesting class of layered compounds, which have attracted much attention due to the discovery of superconductivity with unexpectedly high transition temperatures of 15 K for M=Zr and even up to 25.5 K for M=Hf after intercalation with alkali-metal atoms (Li, Na, K).[1,2] The parent compounds β-MNCl are semiconductors with an optic band gap of 3 to 4 eV.[2] Their crystal structure consists of hexagonal M-N bilayers sandwiched on either side by Cl layers. Each neutral unit $(M\mathrm{NCl})_2$ is only weakly bound to neighboring units by a van der Waals-like interaction. Similar to graphite, this weak interlayer coupling allows intercalation with alkaline elements (Li, Na, K) into the van der Waals gap between two Cl layers, which donates electrons to the MN bilayers rendering them metallic. The doping concentration can be varied over a wide range up to 1.4 alkaline atoms per MNCl formula unit.[3] Recently, electron doping of the bilayers was also achieved by deintercalation of some of the chlorine atoms.[4] In addition, the distance between neighboring $(M\mathrm{NCl})_2$ units can be significantly increased by cointercalation with organic molecules like THF (tetrahydrofuran). By this technique, one can achieve more than a doubling of the interlayer separation, as, e.g., for ZrNCl, from 9.2 Å to 22.4 Å.[3] Thus, in this class of layered compounds, one has good experimental control of two important parameters, the doping level and the interlayer separation, opening the way for a detailed study of their influence on the superconducting properties.

Several electronic structure studies with *ab initio* methods have been devoted to this class of materials.[5–9] With one exception,[6] they all find a two-dimensional electronic structure, with significant covalency in the bonding between N $2p$ states and transition metal d states. The undoped compound is a band insulator with an indirect band gap of 1.5 to 2.5 eV.[5,9] Virtual crystal studies support the idea that each dopant gives away one electron which goes into a conduction band of N p–M d character[7,8] with a large bandwidth of ≈ 1.5 eV, suggesting that correlation effects should be weak. In addition, the calculated Fermi level density of states is found to be small (0.74 states per eV for $Na_{0.25}$HfNCl). A comparable value has been deduced from measurements of the Pauli susceptibility on cointercalated HfNCl.[10]

Studies on Li_xZrNCl have shown that the superconducting transition temperature exhibits a peculiar doping dependence. Superconductivity is observed for $x>0.13$ with $T_c \approx 15$ K. Up to $x=0.5$, T_c hardly changes, while for $x>0.5$, T_c drops monotonously to 10 K for $x=1.4$.[3] A qualitatively similar doping dependence has been observed for the HfNCl compound.[2] Furthermore, T_c seems to be almost insensitive to a change in the interlayer distance.[3] These findings suggest that superconductivity is mainly determined by the properties of an individual MN bilayer. This picture is consistent with NMR and μSR experiments, which found large anisotropies of the penetration depth and coherence length in the superconducting state,[11–13] and is supported by ^{7}Li and ^{35}Cl–NMR measurements on doped HfNCl, which both indicated negligible Fermi-level density of states at the Li and Cl sites, respectively.[11,15]

The identification of the electron-phonon coupling as responsible for the pairing in the 40 K superconductor MgB_2 has proven that in principle phonons can mediate superconductivity with such a high T_c value under favorable conditions. In the case of MgB_2, the main ingredient was the strong coupling of electronic states at the Fermi surface to a high-frequency optic B mode. In MNCl, the presence of light N atoms suggested a similar mechanism. Neutron scattering measurements of the phonon density-of-states[16] and Raman investigations[16,17] identified optic N vibrations in the frequency range of 50 to 90 meV, which is comparable to the B

frequencies in MgB_2. However, no doping-induced softening of these optic modes was observed which would indicate a strong electron-phonon coupling. A recent measurement of the N-isotope coefficient for doped HfNCl gave a surprisingly small value of 0.07.[14] Attempts to get an estimate for the average electron-phonon coupling constant λ from experiments have also led to conflicting results. On the one hand, from a high-pressure study on Raman modes of Cl-deficient ZrNCl and of doped HfNCl a very large coupling of $\lambda \approx 3$ was deduced.[18] On the other hand, the recent analysis of specific heat data for Li-doped ZrNCl suggested a very small value of $\lambda = 0.22$.[19] These contradictions seem to indicate a breakdown of the standard dirty-limit analysis for these layered compounds.

Until now there has been only one attempt to theoretically characterize the strength of the electron-phonon coupling. It was based on the calculation of the Hopfield parameters for $Na_{0.25}HfNCl$ using the Gaspari-Gyorffy approximation and resulted in values of the coupling strength which were one order of magnitude smaller than typically found for binary superconductors with similar T_c.[7] This finding increased doubts that the conventional phonon mechanism is not strong enough to explain the observed T_c and raised the question about alternative pairing mechanism in these layered compounds. As correlation or magnetic pairing mechanism are not very likely, focus has been made on the possible importance of the long-range Coulomb interaction in these layered materials. In 2D systems, the screening of the Coulomb interaction significantly differs to those of 3D metals. The reduced dimensionality gives rise to low-frequency collective modes of the electron system (acoustic plasmons). The possibility of plasmon-mediated pairing in 2D has been investigated in the past.[20,21] In a more realistic model adequate for layered conductors, Bill and coworkers investigated the possibility that the dynamical effects due to this modified screening can cooperate with the phonon coupling, and found a significant enhancement of the pairing interaction due to the contribution of low-frequency plasmons.[22,23]

This paper is devoted to a detailed theoretical investigation of the lattice dynamics and electron-phonon coupling in undoped and Li-doped ZrNCl. The prime goal is to provide reliable information on the phonon dynamics, and an accurate calculation of the electron-phonon interaction using first principles electronic structure methods.

The paper is organized as follows. In Sec. II, details of the applied calculational scheme are outlined. Section III introduces the various structural models and discusses the properties of their electronic structure. The lattice dynamics of both undoped and doped compounds are discussed in Sec. IV. This is followed in Sec. V by an analysis of the electron-phonon interaction, while Sec. VI is devoted to concluding remarks and a summary of the main results.

II. CALCULATIONAL DETAILS

The present calculations of the lattice dynamics and electron-phonon coupling are performed using the linear response technique in combination with the mixed-basis pseudopotential method.[24] The pseudopotential for Zr was constructed according to the description of Bachelet, Hamann, and Schlüter,[25] while for N, Cl, and Li, Vanderbilt-type pseudopotentials were created.[26] For the Li pseudopotential, partial core corrections were taken into account. The Zr and N pseudopotentials have been already used in previous studies.[27,28] The mixed-basis scheme uses a combination of local functions and plane waves for the representation of the valence states,[29,30] which allows for an efficient treatment of the fairly deep d potential for Zr and p potentials for N and Cl. We employed s- and p-type local functions for each N and Cl site, and p- and d-type for each Zr site. Supplementary plane waves were taken into account up to a kinetic energy of 22 Ry. The local-density approximation using the Hedin-Lundqvist form of the exchange-correlation functional[31] was used.

The integration of the rhombohedral Brillouin zone (BZ) has been performed using the smearing technique[32] with a Gaussian broadening of 0.2 eV and hexagonal k-point meshes following the scheme of Moreno and Soler.[33] Sufficient convergence of the ground state and phonon calculations were achieved with a hexagonal $12 \times 12 \times 2$ mesh corresponding to 96 k points in the irreducible wedge of the BZ (IBZ). Phonon dispersions are obtained by standard Fourier interpolation[34,35] from the dynamical matrices calculated on a hexagonal $6 \times 6 \times 2$ grid (32 points in the IBZ). For the analysis of the electron-phonon coupling, a much denser k-point mesh (hexagonal $36 \times 36 \times 2$ or 722 points in IBZ) was necessary to obtain sufficiently converged results.

III. STRUCTURAL MODELS AND ELECTRONIC PROPERTIES

Although the compounds β-ZrNCl and β-HfNCl have been known since 1964,[36] their crystal structures have been long under debate, but are now clarified by recent powder neutron diffraction experiments[37–39] and confirmed by x-ray diffraction studies on single crystals.[40,41] It was found that β-HfNCl is isostructural to β-ZrNCl, and that doping by alkaline elements leads to the same structural changes for both compounds. Therefore, in the following we will only consider Li_xZrNCl for definiteness.

The structure of the insulating parent compound β-ZrNCl is shown in Fig. 1(a). The central structural units are bilayers of ZrN. Each ZrN layer consists of two interconnected honeycomb lattices, which are slightly buckled. Adjacent ZrN layers are shifted such that a short Zr-N interlayer bond exists. Therefore, each Zr (N) is bonded to four neighboring N (Zr), three belonging to the same ZrN layer and one to the adjacent one. Each bilayer is sandwiched between two Cl layers leading to a neutral $(ZrNCl)_2$ unit. The bonding between these neutral units $(ZrNCl)_2$ is of a weak van der Waals type. Neighboring units are shifted relative to each other, resulting in a rhombohedral structure (space group $R\bar{3}m$), with a bilayer stacking period of three original hexagonal unit cells. In the present calculations for undoped β-ZrNCl, the stacking sequence was chosen according to the structural data of Shamoto *et al.*[37] Each primitive unit cell contains two formula units.

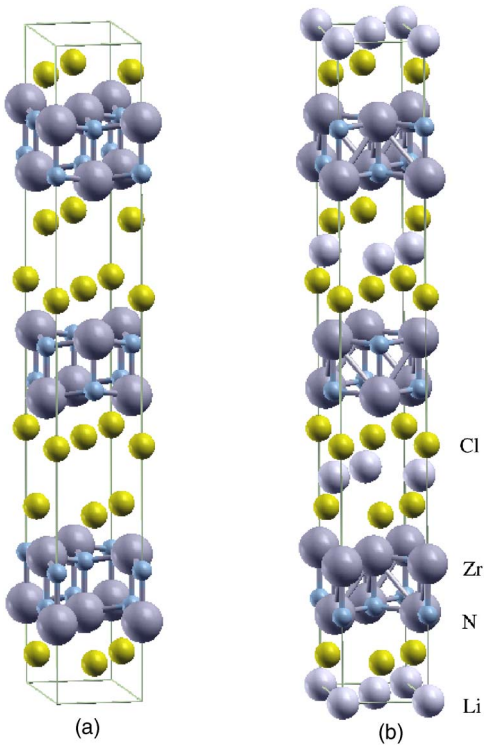

FIG. 1. (Color online) Crystal structures of (a) β-ZrNCl and (b) $Li_{0.5}ZrNCl$ (Ref. 48).

On Li doping, the dopants occupy a high symmetry site (6c) within the van der Waals gap between two Cl layers [see Fig. 1(b)]. The space group is not changed, but the shift between neighboring bilayers is altered, which can be described formally by an exchange of Zr and N. As there is one such 6c site per bilayer, full occupancy corresponds to a doping level of $x=0.5$.

Experimentally, intercalation with Li could be obtained with standard techniques only up to a doping level of $x=0.16$. Higher doping concentrations require the cointercalation with organic molecules, which significantly increases the interbilayer distance. However, the T_c does not change for the range $x=0.16$ to 0.5.[3]

Therefore, in the present study we were concentrating on the doping level $x=1/6$, corresponding to 1/3 occupation of the Li site. To avoid the use of supercells, we took the following approach. An artificial doping is achieved by adjusting the Fermi level until the desired electron count is reached. Charge neutrality in the unit cell is restored by a compensating background charge. The electron charge density is obtained self-consistently. Our starting point is the geometry of $Li_{0.16}ZrNCl$ as obtained by Shamoto *et al.*[37] To verify the applicability of this procedure, we are comparing two model structures:

(A) Without Li, but with 1/3 electrons per unit cell added to simulate Li doping with $x=1/6$. The structure differs to the structure of β-ZrNCl by a different stacking sequence of the $(ZrNCl)_2$ units.

(B) One Li per unit cell (full occupancy), but with 2/3 electrons per unit cell removed to reach the same doping level of $x=1/6$.

Thus both structures correspond to a doping level of $x=1/6$. Comparing them allows us to address the question to what extent the Li dopants can be considered to merely act as donors without significant influence on the electronic properties and the electron-phonon coupling.

All structures were fully relaxed with respect to their three internal structural parameters. For β-ZrNCl both lattice parameters were optimized. In the case of the doped systems, only the in-plane lattice constants have been optimized, while c was kept at the experimental value of $Li_{0.16}ZrNCl$.[37] Results of the structural optimization are given in Table I. The optimized internal structural parameters agree reasonably well with the experimental observations. In all cases, we found a slight expansion of the lattice constants, with a maximum of 3.5% for the doped structure A. This deviation is, however, still in the range of variations typically found for LDA calculations.

Results of the band structures for the optimized geometries of β-ZrNCl and the two doped model structures A and B are shown in Fig. 2. As the electronic structure exhibits a large degree of two-dimensionality, there is a close similarity to the hexagonal symmetry of a single bilayer. Figure 3 visualizes the path Γ-F-Z'-Γ within the $x-y$ plane.

The two-dimensional character of the band structure is exemplified for β-ZrNCl [Fig. 2(a)]. It is most pronounced

TABLE I. Structural parameters of Li_xZrNCl.

x		a (Å)	c (Å)	c/a	z (Zr)	z (N)	z (Cl)
0	This work	3.6629	28.101	7.6718	0.1190	0.1978	0.3884
	Expt.[a]	3.5974	27.548	7.6578	0.1208	0.1984	0.3876
	Expt.[b]	3.6046	27.672	7.6769	0.1192	0.1977	0.3878
	Expt.[c]	3.6039	27.672	7.6783	0.1194	0.2039	0.3868
1/6	This work, model A	3.7277	(27.694)	7.4292	0.2126	0.1341	0.3889
	This work, model B	3.6862	(27.694)	7.5129	0.2118	0.1329	0.3831
	Expt.[a]	3.6016	27.694	7.6894	0.2076	0.1307	0.3883
	Expt.[d]	3.591	27.839	7.7524	0.2126	0.1362	0.3885

[a] $T=4$ K, neutron powder diffraction, Ref. 37.
[b] $T=298$ K, x-ray single crystal diffraction, Ref. 40.
[c] $T=298$ K, x-ray powder diffraction, Ref. 6.
[d] $x=0.2(1)$, $T=298$ K, x-ray single crystal diffraction, Ref. 41.

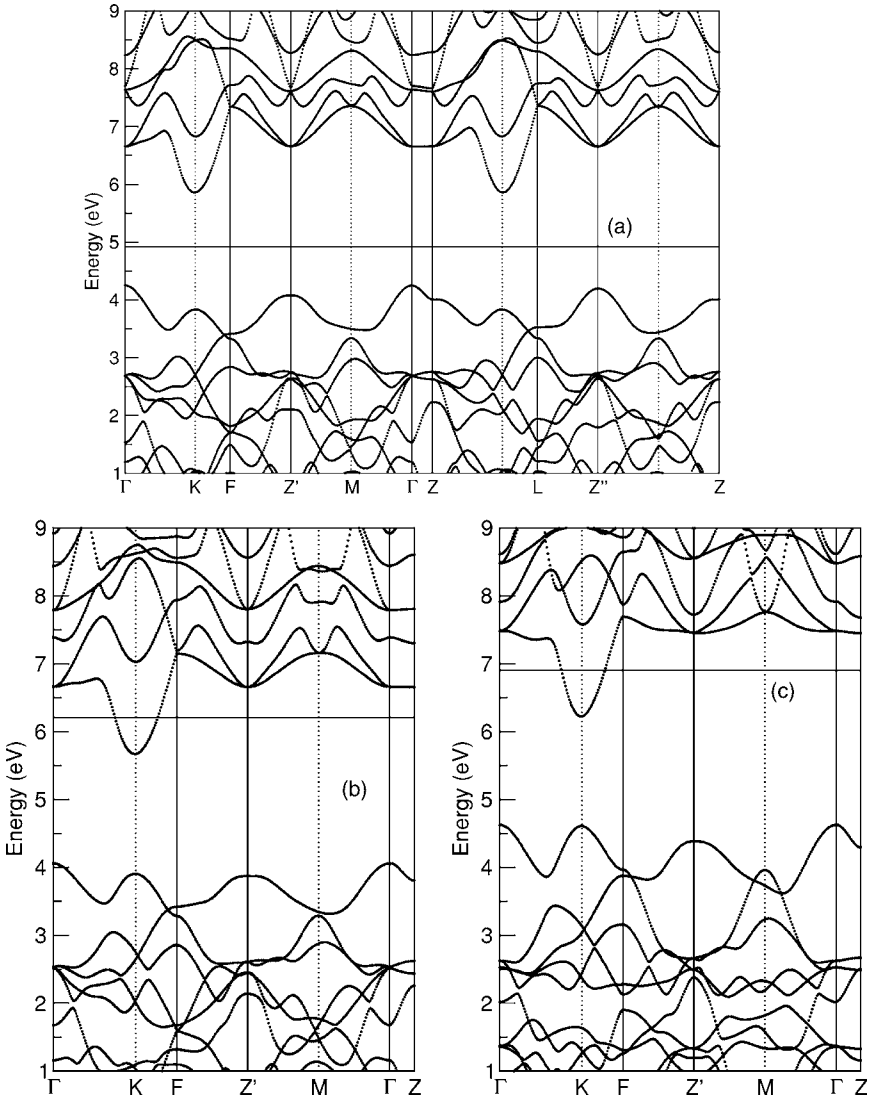

FIG. 2. Band structures for the optimized geometries of β-ZrNCl (a) and of the Li-doped model structures A (b) and B (c). The line Γ-F-Z'-Γ describes the path within the $k_z=0$ plane of the rhombohedral Brillouin zone as defined in Fig. 3. The line Z-L-Z''-Z is the corresponding path obtained by a shift along the rhombohedral axis ($k_z=3\pi/c$).

for the low-lying conduction bands, while some valence bands show small dispersion in c direction. The lowest conduction band possesses its minimum at the K point, leading to an indirect band gap of 1.6 eV.

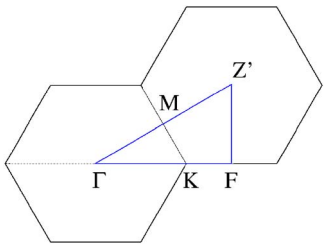

FIG. 3. (Color online) Cut through the rhombohedral Brillouin zone in the $k_z=0$ plane. K and M are not true special points of the rhombohedral BZ, but denote high-symmetry points of the hexagonal BZ of a single bilayer. Z' is equivalent to the point $2/3Z$, where $Z=(0,0,3\pi/c)$ denotes the BZ boundary along the rhombohedral axis. Similarly, F corresponds to the point $M+2/3$ Z. For a true hexagonal structure, F and M, as well as Γ and Z', would have been equivalent.

As illustrated in Figs. 2(b) and 2(c), neither the structural changes due to the different stacking, nor the occupation of the Li site alter significantly the shape of the lowest conduction band. For not too large doping levels, electrons will fill only this single band. The Fermi surface consists of cylinders centered at the K points. Its cross section is a triangularly deformed circle with a radius anisotropy of $\approx 10\%$. The dimensions of the Fermi surface are very similar for the two calculations for models A and B. The band is characterized by a rather small density of states at E_F and a small effective mass m^*. For model A, we find $N(E_F)=0.337$ states per (eV spin cell) and $m^*=0.66\,m$. In the case of full Li site occupancy (model B), the band dispersion is slightly steeper, which results in a reduction of $N(E_F)$ and of m^* by $\approx 10\%$. All these findings are in agreement with previous electronic structure calculations.[5,7–9]

The similarity of the electronic structures in the vicinity of the Fermi energy for empty and full occupation of the Li site (models A and B, respectively) demonstrates that as far as the electronic properties are concerned the Li atoms merely act as donators of electron to the ZrN bilayers, which justifies the artificial doping approach adopted in this work.

TABLE II. Raman active phonons of Li_xZrNCl. The frequencies are given in cm^{-1}.

x		$A_g^{(1)}$	$A_g^{(2)}$	$A_g^{(3)}$	$E_g^{(1)}$	$E_g^{(2)}$	$E_g^{(3)}$
0	This work	182	312	564	114	171	620
	Expt.[a]	187	326	590	123	179	604
	Expt.[b]	191	331	591	128	184	605
	Theory[c]	202	334	586			
1/6	This work, model A	186	303	565	116	169	599
	This work, model B	217	296	548	131	165	633
	Expt.[a]	188	322	582	123	178	608

[a]Adelmann *et al.*, Ref. 16.
[b]Cros *et al.*, Ref. 17.
[c]Weht *et al.*, Ref. 7.

IV. LATTICE DYNAMICS

A. Undoped compound β-ZrNCl

The optic modes of β-ZrNCl at the BZ center can be decomposed into six Raman active modes $(3A_g+3E_g)$ and four infrared active (IR) modes $(2A_{2u}+2E_u)$. The calculated frequencies of Raman modes are collected in Table II and compared with available experimental data. Deviations to measured frequencies are of the order of 5%.

For the insulating compound β-ZrNCl, a complete characterization of its lattice dynamics requires knowledge of the dielectric tensor $\epsilon^{\infty}_{\alpha\beta}$ and Born effective charge tensors $Z^*_{\alpha\beta}(\kappa)$ for each ion κ, which determine the non-analytic contribution to the dynamical matrix in the limit $q \to 0$.[34,35] We extracted the nonanalytic part from calculations for q points close to the center of the BZ along different directions in reciprocal space. In this way, all matrix elements of the dielectric and Born effective charge tensors can be determined except for a single scale factor because only ratios $Z^*/\sqrt{\epsilon^{\infty}}$ enter the expression for the dynamical matrix.

For the rhombohedral lattice, the dielectric tensor is diagonal and has only two independent elements, $\epsilon^{\infty}_{xx}=\epsilon^{\infty}_{yy}$ and ϵ^{∞}_{zz}. Independent elements of the Born effective charge tensors are shown in Table III. We find a significant anisotropy $\epsilon^{\infty}_{xx}/\epsilon^{\infty}_{zz}=2.02$ as well as large anisotropies in the dynamical polarizabilities for both Zr and N, which reflect the very anisotropic screening properties due to the layered structure.

The frequencies of the IR modes are given in Table IV. The largest LO/TO splitting is observed for the high-energy E_u mode, which corresponds to an in-phase motion of the N sublattice against the Zr sublattice within the basal plane. Experimentally, only two of the IR frequencies have been determined. Our calculations suggest that the frequency observed at 529 cm^{-1} should be assigned to the E_u mode rather than to the A_{2u} mode.

TABLE III. Theoretical values for the independent components of the screened Born-effective charge tensor $Z^*_{\alpha\beta}(\kappa)/\sqrt{\epsilon^{\infty}_{zz}}$ for each atom type κ.

Component	Zr	N	Cl
xx	2.69	−2.03	−0.66
zz	1.14	−0.68	−0.46

The generalized phonon density of states (GDOS) of β-ZrNCl has been measured by inelastic neutron scattering.[16] This quantity provides a good test for the accuracy of the present approach, as it probes the phonon spectrum over the whole BZ. Comparison with the theoretical spectrum is given in Fig. 4. Due to the large mass difference between N and the heavy atoms Zr and Cl, the spectrum divides into two separate parts. The modes with frequencies below 40 meV consist of vibrations of Zr and Cl. Because of the small neutron scattering length of Zr (1/9 Cl), the lower part of the GDOS spectrum predominantly reflects the Cl vibrations, which are responsible for the first two main peaks. Zr modes do however contribute to the small third peak near 35 meV. The upper part of the spectrum, which results from the vibrations of the light N atoms, is found to consist of three distinct maxima with spectral-weight ratios 3:1:2, in agreement with the experimental GDOS.

Thus, our theoretical spectrum reproduces all the main features of the experimental one with an overall accuracy of the calculated frequencies of about 5%. There is the general trend that the calculated frequencies in the lower part of the spectrum are too soft, whereas the upper part is obtained too hard, which may indicate an overestimation of the dynamical couplings between N and the heavy atoms by ≈10%.

Figure 5(a) displays the calculated phonon dispersion curves. As the phonon spectrum has a pronounced two-dimensional character, we only show dispersion curves along in-plane directions and along Γ-Z.

B. Li-doped ZrNCl

On doping, two effects on the lattice dynamics can be distinguished. (i) Introduction of charge carriers into the ZrN double layers modifies the covalent Zr-N bonds and the corresponding dynamical couplings. This should affect predominantly Zr and N modes with in-plane polarization. (ii) The presence of Li atoms leads to additional vibrational degrees of freedom which hybridize with the other phonons. The induced changes are expected to be most significant for vibrations parallel to the rhombohedral axis, especially for Cl vibrations. In the present investigation, the first effect is

TABLE IV. IR active phonons of Li_xZrNCl. Given are the TO frequencies in cm^{-1}. The values in brackets represent the LO frequencies.

x		$A_{2u}^{(1)}$	$A_{2u}^{(2)}$	$A_{2u}^{(3)}$	$E_u^{(1)}$	$E_u^{(2)}$	$E_u^{(3)}$
0	This work	257 (272)	597 (630)		155 (179)	547 (680)	
	Expt.[a]		529		165	666?	
1/6	This work, model A	235	612		148	549	
	This work, model B	184	583	314	113	603	262

[a]Adelmann *et al.*, Ref. 16.

mimicked by model A. Model B incorporates both effects, but the changes induced by the presence of Li atoms are exaggerated due to the full occupancy of the Li site.

Experimentally, only slight doping induced shifts of the Raman frequencies have been observed (see Table II). The largest shift exhibits the $A_g^{(3)}$ mode, which softens by 8 cm^{-1}. Theoretical results for models A and B are also shown in Table II. The mere introduction of carriers (model A) induces only small changes in the Raman frequencies. The only exception is $E_g^{(3)}$, which is an in-plane N vibration. Its softening by 21 cm^{-1} reflects the increase of the in-plane lattice constant a (see Table I). The presence of Li atoms (model B) has a more pronounced influence on the Raman modes. Hardening is found for $A_g^{(1)}$, $E_g^{(1)}$, and $E_g^{(3)}$, while softening occurs for the remaining modes. These trends agree with experimental observation, but the magnitude of frequency shifts is exaggerated in all cases.

The changes in the IR frequencies (Table IV) are predicted to be even larger than for the Raman modes. For model B, the presence of Li atoms gives rise to two additional IR modes at 262 and 314 cm^{-1}. Currently, no experimental data are available for comparison.

The effect of doping on the generalized phonon density of states is shown in Fig. 6, together with the experimental GDOS obtained for a sample with doping level $x=1/6$. For comparison with the experimental GDOS, the theoretical spectra have been corrected with respect to the Li contribution to simulate the proper concentration. The Li partial GDOS has been taken from the calculation for model B, and contributes mainly in the frequency range 30–45 meV. The Li vibrations exhibit a stronger hybridization with the Cl vibrations which results in a disappearance of the peak at 25 meV. The experimental spectrum for $Li_{1/6}ZrNCl$ is less structured than for the undoped compound, which may be related to an inhomogeneous distribution of the Li atoms. Overall, the agreement with model B is more favorable than with model A, indicating that for the phonon spectrum hybridization with Li vibrations cannot be neglected.

Phonon dispersion curves for undoped and Li-doped ZrNCl are compared in Fig. 5. The largest modifications introduced by doping are found for the high-frequency branches which develop a steeper dispersion. This is an indication for a significant coupling of these N vibrations to the introduced charge carriers. Comparing model A to model B, additional phonon branches due to the Li atom appear in the upper part of the acoustic spectrum. Also, the filling of the van der Waals gap by the Li atoms significantly increases the stiffness of the acoustic modes with momenta parallel to the rhombohedral axis (Γ-Z). Furthermore, one can observe relative shifts of certain high-frequency N branches, but the shape of the dispersion curves remains very similar.

V. ELECTRON-PHONON COUPLING

In this section we investigate the electron-phonon interaction and the possibility for phonon-mediated superconductivity in the isotropic limit. A basic quantity is the electronic contribution to the linewidth of a phonon mode $(\mathbf{q}\lambda)$

$$\gamma_{\mathbf{q}\lambda} = 2\pi\omega_{\mathbf{q}\lambda} \sum_{\mathbf{k}\nu\nu'} |g^{\mathbf{q}\lambda}_{\mathbf{k}+\mathbf{q}\nu',\mathbf{k}\nu}|^2 \delta(\epsilon_{\mathbf{k}\nu})\,\delta(\epsilon_{\mathbf{k}+\mathbf{q}\nu'}). \qquad (1)$$

Here, $\omega_{\mathbf{q}\lambda}$ is the phonon frequency, and $\epsilon_{\mathbf{k}\nu}$ describes the energy of an electronic state relative to the Fermi energy. g denotes the screened electron-phonon coupling (EPC) matrix element. Within the perturbational approach to the lattice dynamics, g is directly accessible from quantities obtained in the calculation of the dynamical matrix.[42,43] The phonon linewidth enters the expression for the isotropic Eliashberg function

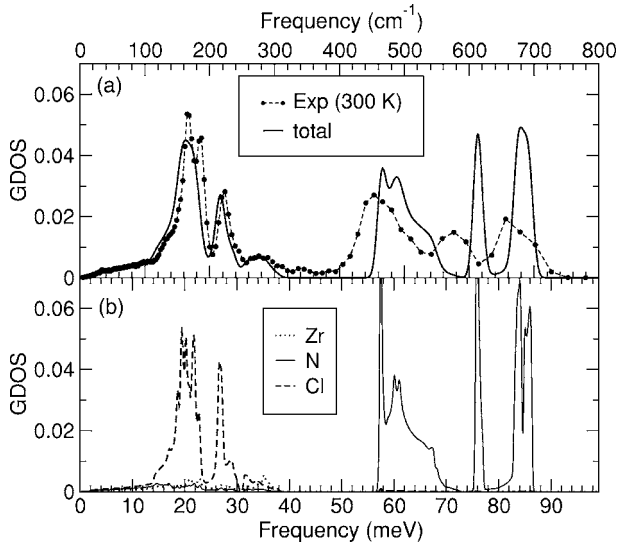

FIG. 4. Generalized density of states of β-ZrNCl. (a) The total GDOS is compared between theory and the experimental data from Ref. 16. Theoretical data have been broadened by 1 meV for a better comparison. (b) Calculated partial GDOS. Here a smaller broadening of 0.1 meV is used to obtain a better resolution of the finer details.

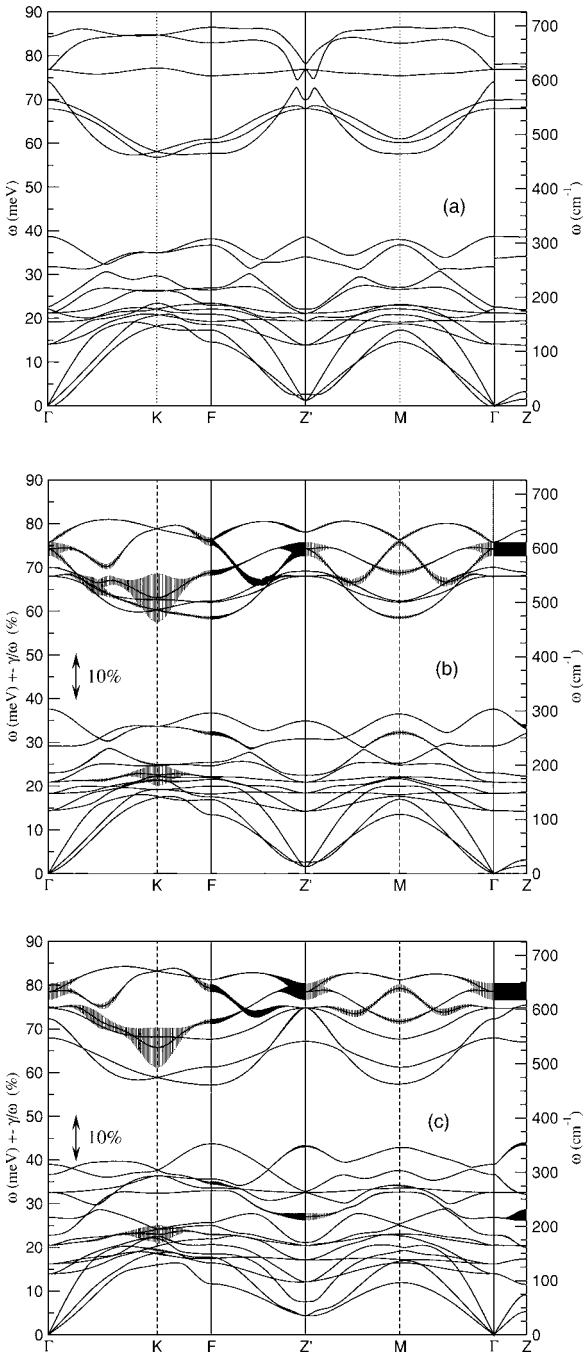

FIG. 5. Phonon dispersions of β-ZrNCl (a) and Li-doped ZrNCl model A (b) and model B (c), respectively. The vertical bars indicate the relative phonon linewidths γ/ω in % as calculated from the electron-phonon coupling [see Eq. (1)].

$$\alpha^2F(\omega) = \frac{1}{2\pi N(E_F)} \sum_{\mathbf{q}\lambda} \frac{\gamma_{\mathbf{q}\lambda}}{\omega_{\mathbf{q}\lambda}} \delta(\omega - \omega_{\mathbf{q}\lambda}), \tag{2}$$

where $N(E_F)$ is the electronic density-of-states (per unit cell and spin) at the Fermi energy. The Eliashberg function determines the average coupling constant

$$\lambda = 2\int_0^\infty d\omega \frac{\alpha^2F(\omega)}{\omega} \tag{3}$$

and an average effective frequency defined as

$$\omega_{\ln} = \exp\left(\frac{2}{\lambda}\int_0^\infty d\omega \frac{\alpha^2F(\omega)}{\omega}\ln(\omega)\right), \tag{4}$$

which sets the energy scale for the superconducting transition temperature.

A good measure for the coupling strength of an individual phonon mode is given by the *relative* linewidth $\gamma_{\mathbf{q}\lambda}/\omega_{\mathbf{q}\lambda}$. In Fig. 5, the relative linewidth is indicated by vertical bars. The following observations can be made: (i) only a few modes exhibit a significant coupling; (ii) the N modes possess a stronger coupling than the acoustic modes; and (iii) very similar EPC is observed for models A and B.

Furthermore, the coupling strength varies significantly as function of momentum. The contribution to λ from all phonon modes at a fixed momentum q, given by

$$\lambda_{\mathbf{q}} = \frac{1}{\pi N(E_F)} \sum_{\lambda} \frac{\gamma_{\mathbf{q}\lambda}}{\omega^2_{\mathbf{q}\lambda}}, \tag{5}$$

has a pronounced maximum at K with a value larger than 2, while in most parts of reciprocal space its value stays below 0.5. As already anticipated by Weht *et al.*,[8] the strong q-dependence of $\lambda_{\mathbf{q}}$ can be traced back to the peculiar shape of the Fermi surface. This behavior can be best understood when considering the quantity

$$\sum_{\mathbf{k}\nu\nu'} \delta(\epsilon_{\mathbf{k}\nu})\delta(\epsilon_{\mathbf{k}+\mathbf{q}\nu'}), \tag{6}$$

which is a measure of the phase space available for scattering of an electron between two states at the Fermi level, whose

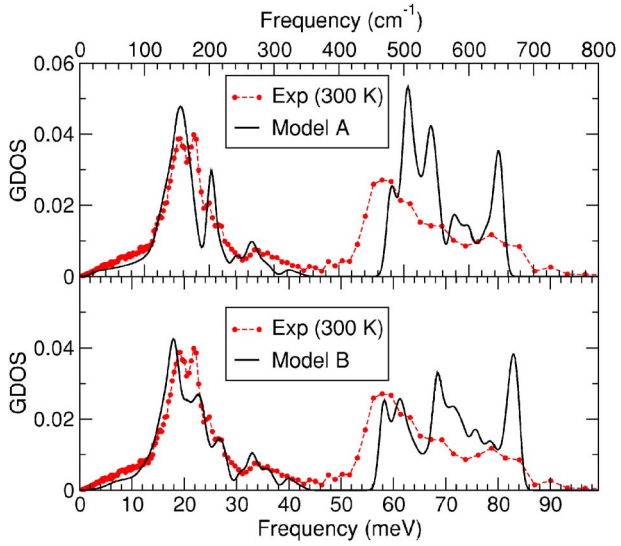

FIG. 6. (Color online) Generalized density of states of $Li_{1/6}$-ZrNCl. (a) The total GDOS is compared between model A and the experimental data from Ref. 16. Theoretical data have been broadened by 1 meV for a better comparison. (b) Same for model B.

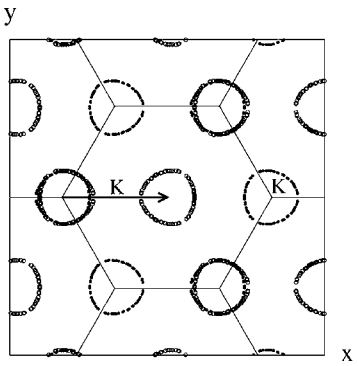

FIG. 7. Cut through the Fermi surface orthogonal to the rhombohedral axis. Full circles indicate the original Fermi surface, open circles the Fermi surface shifted by the momentum K.

momenta differ by $\mathbf{q}$. This quantity becomes large when there is a large overlap of the original Fermi surface and the Fermi surface shifted by a vector $\mathbf{q}$. As indicated in Fig. 7, a large overlap occurs for $\mathbf{q}=K$, where half of the Fermi surface cylinders almost completely overlap. Only the small deformation of the cylinders prevents a perfect overlapping.

The large coupling at K is concentrated almost completely on two specific phonon modes: a Zr mode at $\approx$25 meV and a N vibration at $\approx$ 65 meV. Both vibrations correspond to displacements parallel to the ZrN double layer, which allows an optimal coupling to the conduction states at E_F.

The q-integrated spectral function $\alpha^2F(\omega)$ is displayed in Fig. 8. For model A, large peaks are obtained at $\approx$23 meV and $\approx$65 meV which correspond to the frequencies of the strongly coupled modes at K. The large weight from the optic part of the spectrum indicates a large contribution to the coupling from the N modes. Table V contains some characteristic quantities derived from $\alpha^2F(\omega)$. Despite the small differences in $\alpha^2F(\omega)$, these integrated quantities are very similar for models A and B. We find only a small average coupling constant of $\lambda\approx 0.5$. The optic modes contribute about 45% to λ. The contributions from Cl and Li (model B only) vibrations amount to less than 3% of the total coupling constant, which is consistent with NMR findings for doped HfNCl.[11,15]

From a recent measurement of the linear coefficient γ_n of the electronic specific heat of Li-doped ZrNCl, an upper

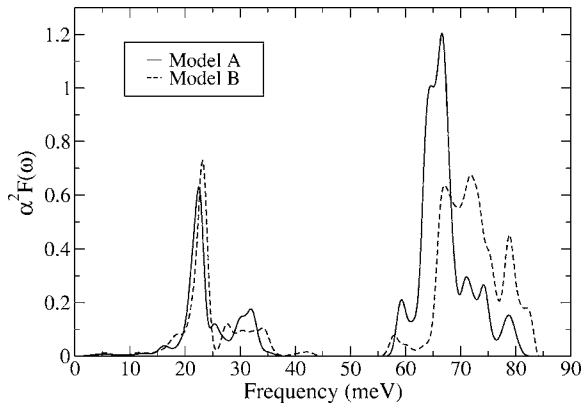

FIG. 8. Calculated Eliashberg functions $\alpha^2F(\omega)$ for $Li_{1/6}ZrNCl$. The spectra are broadened with Gaussians of width 1 meV.

TABLE V. Density of states $N(E_F)$ at the Fermi energy [in states per (eV spin cell)], average coupling constant λ, and effective average phonon frequency $\omega_{\ln}$ (in meV).

Model	$N(E_F)$	λ	$\omega_{\ln}$
A	0.337	0.521	36.4
B	0.291	0.508	35.8

limit of $\lambda=0.22$ has been inferred. This estimate was derived using a lower limit of 0.38 states per (eV spin cell) for the band structure $N(E_F)$ as taken from the literature. In the present calculation, we find significantly smaller values for $N(E_F)$, so that our calculated value of $\lambda\approx 0.5$ is still compatible with the measured γ_n.[19]

To get an estimate for T_c, we have numerically solved the linearized gap equations in the dirty limit using the calculated $\alpha^2F(\omega)$ and taking the Coulomb pseudopotential μ^* as a free parameter.[44] Results are plotted in Fig. 9(a). Values for T_c near the experimentally observed transition temperature of 15 K can only be achieved for very small μ^*. For a value $\mu^*=0.1$ which is typical for normal metals, the predicted T_c is of the order of 5 K and thus much smaller than the experimental T_c.

We have also investigated the isotope effect within the dirty limit. The partial isotope coefficient is defined as

$$\alpha_i = -\frac{d\ln T_c}{d\ln M_i} \approx -\frac{M_i \Delta T_c}{T_c \Delta M_i} \tag{7}$$

for atom type i. A recent measurement of the N-isotope coefficient for Li-doped HfNCl has given a rather small value of $\alpha_N=0.07\pm0.02$. As can be seen from Fig. 9(b), such values can be achieved only for large values of μ^*, where the predicted T_c is too small.

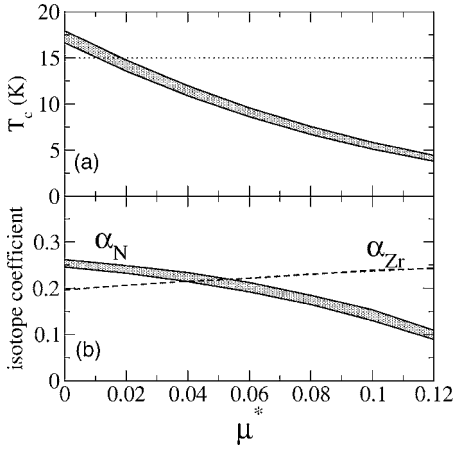

FIG. 9. Estimate of (a) transition temperature T_c and (b) partial isotope coefficients for $Li_{1/6}ZrNCl$ in the dirty limit. The borders of the shaded areas represent the results obtained for model A and B, respectively. For α_{Zr}, they are practically identical. In panel (a), the dashed horizontal line denotes the observed transition temperature.

VI. CONCLUSIONS AND SUMMARY

The first principles analysis presented in the previous sections indicates that the layered structure of doped ZrNCl results in a prominent 2D character of the electronic structure near the Fermi level, of the phonon dispersions, and of the electron-phonon coupling. In accordance with previous theoretical work on Na-intercalated HfNCl,[8] the 2D nature of the conduction band implies that $N(E_F)$ stays practically constant with increasing doping level until a critical doping level of $x_c \approx 0.3$, where a second conduction band starts to be filled. Within the phonon scenario for superconductivity, the constant $N(E_F)$ for $x < x_c$ could explain an almost doping-independent $T_c(x)$ if the average EPC does not change much with band filling. However, our dirty-limit analysis suggests that in this doping regime the EPC is too weak to account for the observed T_c, although the EPC is found to be significantly larger than estimated before.

To solve this apparent contradiction, Pickett has argued that in the low-doping regime, sample inhomogeneities could lead to spacial variations of the doping level.[45] The observed superconductivity is then attributed to the regions with $x > x_c$, where the Fermi level is supposed to lie in a rather flat band with high $N(\mathrm{E}_F)$. This band involves d_z orbitals, it is much more 3D-like, and may support a larger EPC. However, this explanation seems to be at variance with susceptibility measurements, which suggest a rather low $N(E_F)$,[10] as well as with spectroscopic studies on Na-intercalated HfNCl, which found a highly 2D nature of the conduction states.[46,47]

Our estimate of T_c rests on the dirty-limit approximation. As the EPC shows strong q-dependence one may wonder if gap anisotropy may be of importance. In principle anisotropy could lead to an enhanced T_c, but the expected change is typically of the order of a few percent, while our estimate is off by a factor 2–3. Also the presence of only a single conduction band excludes the possibility of a higher T_c due to multiband superconductivity like in MgB_2.

A more likely shortcoming of our analysis is the treatment of the electron-electron interaction by the standard parameter μ^*. The layered crystal structure of ZrNCl consists of alternating conducting and insulating layers. Bill *et al.* have argued that in such a case, the dynamics of the Coulomb screening becomes important.[22,23] The layered structure gives rise to low-lying collective modes of the electrons, which can contribute constructively to the pairing interaction. Based on a simplified model calculation adapted to doped HfNCl, they indeed found a drastic enhancement of T_c due to these dynamical screening effects. These findings suggest that for layered superconductors a more explicit treatment of the dynamical Coulomb interaction in the Eliashberg analysis is required.

In summary, we have presented a first principles study of the lattice dynamics and electron-phonon coupling of undoped and Li-doped ZrNCl. The theoretical phonon spectra are found to be in good agreement with those obtained by neutron scattering experiments. By comparing two limiting structural models, we show that the artificial doping approach is adequate to simulate the effect of intercalation on the electronic structure as well as on the electron-phonon coupling. Despite a large coupling to high-frequency N modes, the average coupling constant is found to be only ≈ 0.5. Therefore, the standard Eliashberg analysis in the dirty limit fails to explain the observed superconducting properties. The peculiar properties of the electron-phonon coupling, namely its quasi-2D character and its strong momentum dependence, hint to a breakdown of the conventional treatment of the electronic screening for these layered materials. The answer to the question of whether transition metal chloronitrides are phonon mediated superconductors or not has to wait for an adequate treatment of the Coulomb interaction in the theory of superconductivity in strongly layered conductors.

*Corresponding author. Fax: +49-724782-4624. Email address: heid@ifp.fzk.de

[1] S. Yamanaka, H. Kawaji, and K. Hotehama, Adv. Mater. (Weinheim, Ger.) **8**, 771 (1996).
[2] S. Yamanaka, K. Hotehama, and H. Kawaji, Nature (London) **392**, 580 (1998).
[3] H. Kawaji, K. Hotehama, and S. Yamanaka, Chem. Mater. **9**, 2127 (1997).
[4] S. Yamanaka, L. Zhu, X. Chen, and H. Tou, Physica B **328**, 6 (2003).
[5] C. Felser and R. Seshadri, J. Mater. Chem. **9**, 459 (1999).
[6] S. Ya. Istomin, J. Köhler, and A. Simon, Physica C **319**, 219 (1999).
[7] R. Weht, A. Filippetti, and W. E. Pickett, Europhys. Lett. **48**, 320 (1999).
[8] R. Weht, A. Filippetti, and W. E. Pickett, in *High Temperature Superconductivity, Proceedings of the Miami HTS99*, AIP Conf. Proc. No. 483 (AIP, New York, 1999), p. 366.
[9] I. Hase and Y. Nishihara, Phys. Rev. B **60**, 1573 (1999).
[10] H. Tou, Y. Maniwa, T. Koiwasaki, and S. Yamanaka, Phys. Rev. Lett. **86**, 5775 (2001).
[11] H. Tou, Y. Maniwa, T. Koiwasaki, and S. Yamanaka, Phys. Rev. B **63**, 020508(R) (2000).
[12] Y. J. Uemura, Y. Fudamoto, I. M. Gat, M. I. Larkin, G. M. Luke, J. Merrin, K. M. Kojima, K. Itoh, S. Yamanaka, R. H. Heffner, and D. E. MacLaughlin, Physica B **289–290**, 389 (2000).
[13] T. Ito, Y. Fudamoto, A. Fukaya, I. M. Gat-Malureanu, M. I. Larkin, P. L. Russo, A. Savici, Y. J. Uemura, K. Groves, R. Breslow, K. Hotehama, S. Yamanaka, P. Kyriakou, M. Rovers, G. M. Luke, and K. M. Kojima, Phys. Rev. B **69**, 134522 (2004).
[14] H. Tou, Y. Maniwa, and S. Yamanaka, Phys. Rev. B **67**, 100509(R) (2003).
[15] H. Tou, Y. Maniwa, S. Yamanaka, and M. Sera, Physica B **329–333**, 1323 (2003).
[16] P. Adelmann, B. Renker, H. Schober, M. Braden, and F. Fernandez-Dias, J. Low Temp. Phys. **117**, 449 (1999).
[17] A. Cros, A. Cantarero, D. Beltrán-Porter, J. Oró-Solé, and A.

Fuertes, Phys. Rev. B **67**, 104502 (2003).
[18] Y. Taguchi, M. Hisakabe, Y. Ohishi, S. Yamanaka, and Y. Iwasa, Phys. Rev. B **70**, 104506 (2004).
[19] Y. Taguchi, M. Hisakabe, and Y. Iwasa, Phys. Rev. Lett. **94**, 217002 (2005).
[20] H. Rietschel and L. J. Sham, Phys. Rev. B **28**, 5100 (1983).
[21] Y. Takada, J. Phys. Soc. Jpn. **45**, 786 (1978).
[22] A. Bill, H. Morawitz, and V. Z. Kresin, J. Supercond. **15**, 483 (2002).
[23] A. Bill, H. Morawitz, and V. Z. Kresin, Phys. Rev. B **68**, 144519 (2003).
[24] R. Heid and K.-P. Bohnen, Phys. Rev. B **60**, R3709 (1999).
[25] G. B. Bachelet, D. R. Hamann, and M. Schlüter, Phys. Rev. B **26**, 4199 (1982).
[26] D. Vanderbilt, Phys. Rev. B **32**, 8412 (1985).
[27] M. Yamamoto, M. Kurahashi, C. T. Chan, K. M. Ho, and S. Naito, Surf. Sci. **387**, 300 (1997).
[28] R. Heid, K.-P. Bohnen, B. Renker, T. Wolf, and H. Schober, Phys. Rev. B **71**, 092302 (2005).
[29] S. G. Louie, K.-M. Ho, and M. L. Cohen, Phys. Rev. B **19**, 1774 (1979).
[30] B. Meyer, C. Elsässer, and M. Fähnle, FORTRAN90 Program for Mixed-Basis Pseudopotential Calculations for Crystals, Max-Planck-Institut für Metallforschung, Stuttgart (unpublished).
[31] L. Hedin and B. J. Lundqvist, J. Phys. C **4**, 2064 (1971).
[32] C.-L. Fu and K. M. Ho, Phys. Rev. B **28**, 5480 (1983).
[33] J. Moreno and J. M. Soler, Phys. Rev. B **45**, 13891 (1992).
[34] P. Giannozzi, S. de Gironcoli, P. Pavone, and S. Baroni, Phys. Rev. B **43**, 7231 (1991).
[35] X. Gonze and C. Lee, Phys. Rev. B **55**, 10355 (1997).
[36] R. Juza and H. Friedrichsen, Z. Anorg. Allg. Chem. **332**, 159 (1964); **332**, 173 (1964).
[37] S. Shamoto, T. Kato, Y. Ono, Y. Miyazaki, K. Ohoyama, M. Ohashi, Y. Yamaguchi, and T. Kajitani, Physica C **306**, 7 (1998).
[38] S. Shamoto, K. Iizawa, M. Yamada, K. Ohoyama, Y. Yamaguchi, and T. Kajitani, J. Phys. Chem. Solids **60**, 1431 (1999).
[39] S. Shamoto, K. Takeuchi, S. Yamanaka, and T. Kajitani, Physica C **402**, 283 (2004).
[40] X. Chen, T. Koiwasaki, and S. Yamanaka, J. Solid State Chem. **159**, 80 (2001).
[41] X. Chen, L. Zhu, and S. Yamanaka, J. Solid State Chem. **169**, 149 (2002).
[42] S. Y. Savrasov, D. Y. Savrasov, and O. K. Andersen, Phys. Rev. Lett. **72**, 372 (1994).
[43] R. Heid, L. Pintschovius, W. Reichardt, and K.-P. Bohnen, Phys. Rev. B **61**, 12059 (2000).
[44] G. Bergmann and D. Rainer, Z. Phys. **263**, 59 (1973).
[45] W. E. Pickett, Physica B **296**, 112 (2001).
[46] T. Yokoya, Y. Ishiwata, S. Shin, S. Shamoto, K. Iizawa, T. Kajitani, I. Hase, and T. Takahashi, Phys. Rev. B **64**, 153107 (2001).
[47] T. Takeuchi, S. Tsuda, T. Yokoya, T. Tsukamoto, S. Shin, A. Hirai, S. Shamoto, and T. Kajitani, Physica C **392–396**, 127 (2003).
[48] *XCrySDen* is a new program for displaying crystalline structures and electron densities. A. Kokalj, J. Mol. Graphics Modell. **17**, 176 (1999). Code is available from http://www.xcrysden.org/.